





Arabidopsis Sec14 proteins (SFH5 and SFH7) mediate interorganelle transport of phosphatidic acid and regulate chloroplast development

Hong-Yan Yao^{a,b,1}, Yao-Qi Lu^{c,1}, Xiao-Li Yang^{b,1}, Xiao-Qing Wang^c, Zhipu Luo^c, De-Li Lin^d, Jia-Wei Wu^{c,2} , and Hong-Wei Xue^{d,2} 

Edited by Xuemin Wang, University of Missouri-St Louis, St. Louis, MO; received December 28, 2022; accepted January 9, 2023 by Editorial Board Member Joseph J. Kieber

Lipids establish the specialized thylakoid membrane of chloroplast in eukaryotic photosynthetic organisms, while the molecular basis of lipid transfer from other organelles to chloroplast remains further elucidation. Here we revealed the structural basis of *Arabidopsis* Sec14 homology proteins AtSFH5 and AtSFH7 in transferring phosphatidic acid (PA) from endoplasmic reticulum (ER) to chloroplast, and whose function in regulating the lipid composition of chloroplast and thylakoid development. AtSFH5 and AtSFH7 localize at both ER and chloroplast, whose deficiency resulted in an abnormal chloroplast structure and a decreased thickness of stacked thylakoid membranes. We demonstrated that AtSFH5, but not yeast and human Sec14 proteins, could specifically recognize and transfer PA in vitro. Crystal structures of the AtSFH5-Sec14 domain in complex with L- α -phosphatidic acid (L- α -PA) and 1,2-dipalmitoyl-sn-glycero-3-phosphate (DPPA) revealed that two PA ligands nestled in the central cavity with different configurations, elucidating the specific binding mode of PA to AtSFH5, different from the reported phosphatidylethanolamine (PE)/phosphatidylcholine (PC)/phosphatidylinositol (PI) binding modes. Quantitative lipidomic analysis of chloroplast lipids showed that PA and monogalactosyldiacylglycerol (MGDG), particularly the C18 fatty acids at *sn*-2 position in MGDG were significantly decreased, indicating a disrupted ER-to-plastid (chloroplast) lipid transfer, under deficiency of AtSFH5 and AtSFH7. Our studies identified the role and elucidated the structural basis of plant SFH proteins in transferring PA between organelles, and suggested a model for ER-chloroplast interorganelle phospholipid transport from inherent ER to chloroplast derived from endosymbiosis of a cyanobacterium providing a mechanism involved in the adaptive evolution of cellular plastids.

SFH protein | chloroplast development | PA transfer | ER-chloroplast interorganelle | structural basis

The photosynthetic transform of light energy into chemical potential establishes the energy sources for life survival on earth. Chloroplast, a double-membrane organelle derived from endosymbiosis of a cyanobacterium, provides the structural basis of photosynthesis. Thylakoids are folded by internal membrane of chloroplasts and own the unique membrane structure assembled by lipids, enzymes, and pigments (1). Thylakoid membranes are composed to a large amount of galactoglycerolipids [including monogalactosyldiacylglycerol (MGDG) and digalactosyldiacylglycerol (DGDG)], which establish the specific and functional membranes and are integral constituents of photosynthetic complexes (1). Transfer of lipids from endoplasmic reticulum (ER) is crucial for lipid biosynthesis of thylakoid membrane, and defective biosynthesis of MGDG and DGDG or transfer of lipids has detrimental effects on thylakoid biogenesis and chloroplast development, leading to decreased chlorophyll content, abnormal chloroplast ultrastructure, and reduced photosynthetic activity (2, 3). *Arabidopsis* trigalactosyldiacylglycerol (TGD) machinery that consists of TGD1 (permease), TGD2 (PA binding) and TGD3 (ATPase) proteins plays essential role in lipid transfer from ER to plastids or from outer envelope and intermembrane space to the stromal side of inner envelope membrane of chloroplasts (4–7), and disruption of each TGD member all caused the abnormal biosynthesis of ER-derived thylakoid lipids.

More than 20 lipid transfer protein (LTP) families have been identified in the human, yeast, and planta, which transfer various lipids between membranes in a nonvesicular manner (8). Proteins of relevant evolutionary and lymphoid interest (PRELI) is capable of binding and transporting phosphatidic acid (PA) between subcellular compartments (9). Human RdgB proteins of phosphatidylinositol transfer protein family bind and transfer PA; in particular, RdgB α 1/Nir2 transfers PA from the plasma membrane to ER while delivering PI in the opposite direction (10, 11). The yeast Ups1-Mdm35 complex of PRELI family

Significance

Solar is converted to chemical energy at thylakoid membranes of eukaryotic photosynthetic organisms, and proper lipid assembly in thylakoid membrane, particularly the transfer of lipid precursors from other organelles, is crucial. Sec14 homology proteins are identified in all eukaryotes, which can bind and transfer a wide range of lipids. By crystallizing the Sec14 domain of *Arabidopsis* Sec14 homology protein5 (AtSFH5) and relevant biochemical and genetic studies, we elucidated the specific binding modes of phosphatidic acid (PA) and unique structural features of plant Sec14 domains, and demonstrated the crucial roles of AtSFH5 and AtSFH7 in regulating chloroplast development providing a model for interorganelle phospholipid transport and a mechanism involving in the adaptive evolution of cellular plastids.

Author contributions: J.-W.W. and H.-W.X. designed research; H.-Y.Y., Y.-Q.L., X.-L.Y., X.-Q.W., Z.L., and D.-L.L. performed research; H.-Y.Y., Y.-Q.L., X.-L.Y., X.-Q.W., Z.L., D.-L.L., J.-W.W., and H.-W.X. analyzed data; and H.-Y.Y., Y.-Q.L., J.-W.W., and H.-W.X. wrote the paper.

The authors declare no competing interest.

This article is a PNAS Direct Submission. X.W. is a guest editor invited by the Editorial Board.

Copyright © 2023 the Author(s). Published by PNAS. This open access article is distributed under Creative Commons Attribution-NonCommercial-NoDerivatives License 4.0 (CC BY-NC-ND).

¹H.-Y.Y., Y.-Q.L., and X.-L.Y. contributed equally to this work.

²To whom correspondence may be addressed. Email: jiaweiwu@suda.edu.cn or hwxue@sjtu.edu.cn.

This article contains supporting information online at <https://www.pnas.org/lookup/suppl/doi:10.1073/pnas.2221637120/-/DCSupplemental>.

Published January 30, 2023.

binds PA at the outer membrane of mitochondria and transfers it to the inner membrane (12, 13). Nevertheless, it remains elusive which LTPs in planta can transfer PA between organelles.

The Sec14 family is identified in all eukaryotes and characterized by a conserved Sec14 domain that can bind and transfer a wide range of lipids and hydrophobic vitamins *in vitro* (14). The *Saccharomyces cerevisiae* genome encodes prototype Sec14p and five Sec14 homologues (designated Sfh1p-Sfh5p) that exhibit various physiological functions in lipid metabolism and membrane trafficking (15). There are ~30 Sec14-containing proteins in *Homo sapiens*, and dysfunctions of them would cause a number of diseases such as vitamin E deficiency, autosomal-dominant cancers, and ataxia (14). All yeast Sec14 proteins contain one Sec14 domain, while most human Sec14 members are complex modular proteins comprising additional domains including Golgi dynamics (GOLD), pleckstrin homology (PH), and protein kinase/phosphatase. There are 32 Sec14 members in *Arabidopsis thaliana*, which can be subdivided into three subfamilies, the Sec14 alone members (AtPITP1-12), the Sec14-GOLD proteins (patellins, AtPATL1-6), and plant-specific members Sec14-Nodulin proteins (AtSFH1-14) (16).

PA, the key lipid precursor of thylakoid membrane assembly, is mainly synthesized at ER, and synthesis of diacylglycerol (DAG), successive PG-phosphate and phosphatidylglycerol (PG) (17), and then galactolipids [MGDG, DGDG, and sulfoquinovosyldiacylglycerol (SQDG)] in thylakoid membrane of chloroplast relies on PA (18). Studies showed that TGD machinery involved in ER to thylakoid lipid transfer in *Arabidopsis* (4); however, how PA traffics from ER or other membrane structures to outer envelope of chloroplast remains further understood. Through the systemic genetic, structural, and lipidomic analysis, we here functionally characterized and elucidated the molecular basis and importance of ER-chloroplast PA transport in plant cells. AtSFH5 and AtSFH7 localize at ER and chloroplast, and efficiently transfer PA between membranes. Crystal structures of AtSFH5 in complex with different PA ligands revealed that PA binds deeply in the hydrophobic pocket of the Sec14 domain. The binding mode of PA to AtSFH5 is similar to, yet different from the reported PE/PC/PI binding ones.

Results

***Arabidopsis* AtSFH5 and AtSFH7 Are Crucial for Photoautotrophic Growth and Chloroplast Development.** To study the function of plant-specific SFH protein subfamily, the eFP Browser (http://bar.utoronto.ca/efp_arabidopsis/cgi-bin/efpWeb.cgi) was searched and *AtSFH5* and *AtSFH7* genes with similar expression patterns were selected. Real-time quantitative polymerase chain reaction (qPCR) analysis showed that both *AtSFH5* and *AtSFH7* were transcribed in various tissues and highly expressed in leaves (SI Appendix, Fig. S1A). Promoter-reporter (β -glucuronidase, GUS) fusion analysis by observing transgenic seedlings showed that *AtSFH5* and *AtSFH7* were mainly expressed in cotyledons and rosette leaves at different developmental stages (SI Appendix, Fig. S1B), suggesting a role of *AtSFH5* and *AtSFH7* during vegetative growth.

Transferred DNA (T-DNA) insertional mutants, *sfh5* (SALK_114805C) and *sfh7* (SALK_113006C), were identified (SI Appendix, Fig. S2A). PCR amplification using primers at T-DNA and flanked genomic DNA and qPCR analysis confirmed the T-DNA insertions and deficient transcription of *AtSFH5* and *AtSFH7* (SI Appendix, Fig. S2 B and C). Phenotypic observations showed that there was no obvious growth abnormality of *sfh5* or *sfh7* single mutant, while *sfh5 sfh7* double mutant was semi-dwarf with smaller and pale green rosette leaves (Fig. 1A and SI Appendix, Fig. S3A). Measurement revealed a reduced chlorophyll amount of *sfh5 sfh7* [1.04 mg/g, compared with 1.45 mg/g of Columbia-0

(Col-0)] (Fig. 1B), and a consistently significantly decreased non-photochemical quenching (NPQ, SI Appendix, Fig. S3B). Further analysis of chloroplast's ultrastructure using Transmission Electron Microscope (TEM) showed the severely defective/underdeveloped chloroplasts, which were much smaller in size with a flatter shape, of *sfh5 sfh7* (Fig. 1C). In addition, the thylakoid membrane stacks were notably distorted with an obvious decrease (no highly stacked thylakoid membranes were observed) in *sfh5 sfh7* (Fig. 1C), which might affect the electron transport and chlorophyll synthesis, leading to decreased NPQ. Complemented expression of *AtSFH7* driven by own native promoter in *sfh5 sfh7* resulted in the rescued chloroplast and restored growth (Fig. 1A and SI Appendix, Fig. S3C), confirming the crucial role of *AtSFH5* and *AtSFH7* in chloroplast development and vegetative growth.

AtSFH5 Binds and Transfers PA *In Vitro*. To investigate the ligand specificity, we recombinantly expressed the full-length and variable fragments of AtSFH5 and AtSFH7 in *Escherichia coli*, and only obtained a soluble fragment containing the predicted Sec14 domain of AtSFH5 (AtSFH5-Sec14, residues 76 to 365) (Fig. 2A). We first carried out the protein-lipid overlay assay and found that the recombinant AtSFH5-Sec14 could interact with two species of PA and phosphatidylinositol bis- and tris-phosphates (Fig. 2B). The Sec14 family proteins of yeast and human have been shown to bind and transport PI and phosphatidylcholine (PC) molecules (19, 20); however, the overlay assay did not show the interaction of AtSFH5-Sec14 with these phospholipids (Fig. 2B).

Saccharomyces cerevisiae ScSec14p has been shown to bind PC through a binding assay using fluorophore 7-nitrobenz-2-oxa-1,3-diazole (NBD)-labeled PC (21). We then examined the binding of NBD-PC to plant, human, and yeast Sec14 domains, and found that AtSFH5-Sec14 could bind NBD-PC (SI Appendix, Fig. S4A). In a similar assay using NBD-PA (18:1/12:0-NBD), adding of AtSFH5-Sec14 significantly increased NBD fluorescence, and the more dramatic change(s) upon addition indicated that AtSFH5-Sec14 exhibited higher affinity for PA (and PC) than ScSec14p and ScSfh1p (Fig. 2C). Notably, the *H. sapiens* HsSec14L2-Sec14 domain might bind neither PC nor PA. Since the acyl chain (*sn*-1/2) compositions of chloroplast PAs are mainly palmitic acid (16:0) and unsaturated C18 fatty acid, another NBD-PA (16:0/12:0) was tested, which could also weakly bind to AtSFH5 (SI Appendix, Fig. S4B). Therefore, AtSFH5 can bind different species of chloroplast PAs, yet the acyl chain composition might affect their binding affinities.

To determine the binding affinity, the titration experiment was performed by adding aliquots of AtSFH5-Sec14 protein into the solution containing 2 μ M NBD-PA (Fig. 2D). Unexpectedly, the degree of binding increased linearly with increasing AtSFH5-Sec14 concentration and then reached a plateau at ~0.5 μ M protein concentration. This feature indicated that the experiment was carried out under stoichiometric binding conditions (i.e., the total lipid concentration was at least 10 times greater than the apparent dissociation constant). Notably, the intersection of the increase slope in fluorescence with the maximum value gives the stoichiometry of the protein-lipid complex, and the efficient amount of NBD-PA in solution was estimated to be ~0.48 μ M (an accessibility of approximate 25%). Thus, the binding of AtSFH5-Sec14 to PA was very tight, with an estimated dissociation constant lower than 0.05 μ M.

As PA mainly locates at cellular membranes, we set up a liposome-based PA binding/extraction assay (Fig. 2E). Fluorescent signal of NBD-PA embedded in liposomes could be quenched due to fluorescence resonance energy transfer with 1,2-dipalmitoyl-*sn*-glycero-3-phosphoethanolamine-N-(lissamine rhodamine B sulfonyl)-PE (Rhod-PE), and NBD signal would be dequenched

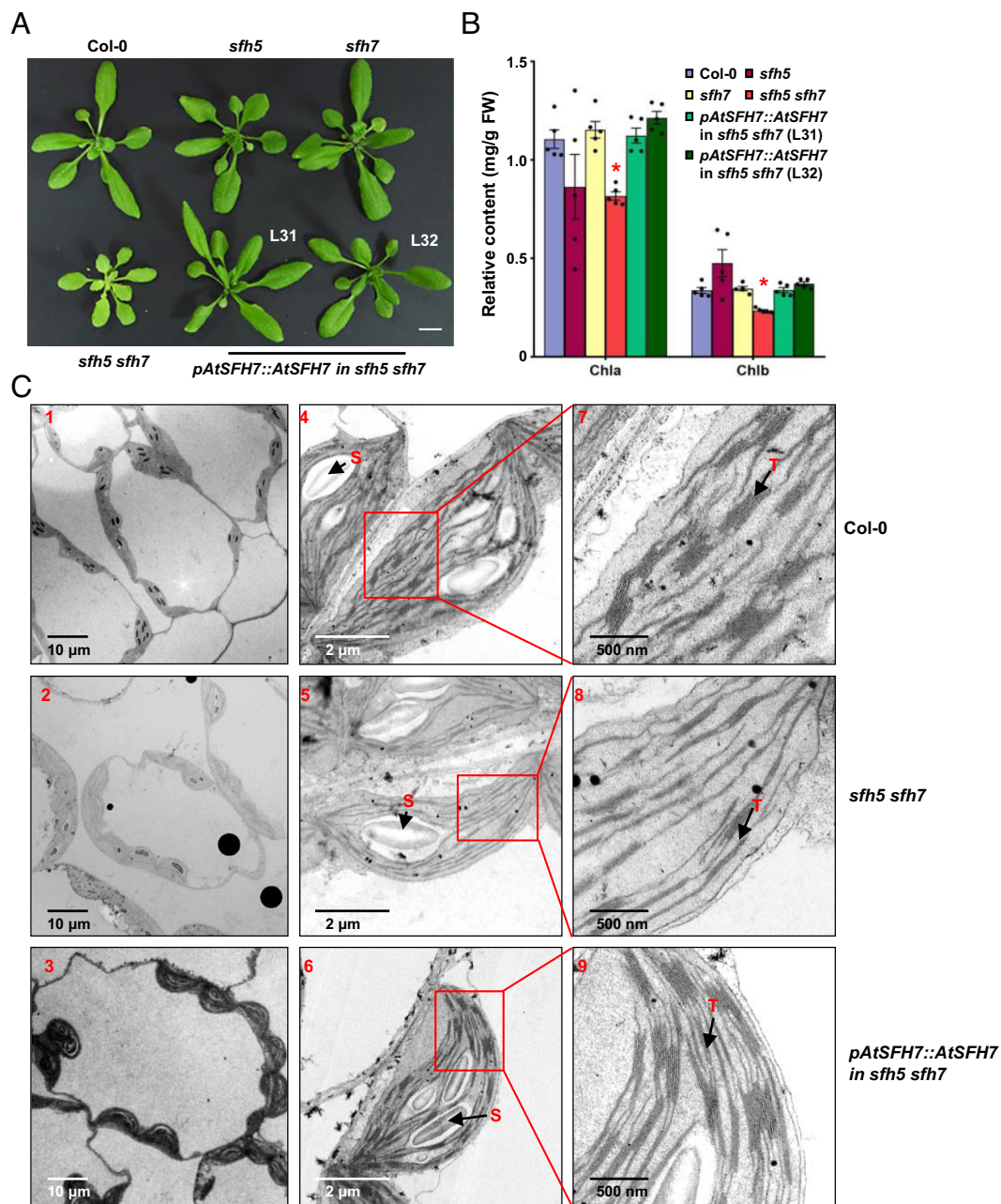


Fig. 1. Defective thylakoid development under deficiencies of AtSFH5 and AtSFH7. (A) Double-mutant *sfh5 sfh7* presents pale yellow leaves, which is recovered by complemented expression of *AtSFH7*. Twenty-three-d-old seedlings were observed and representative images were shown. L31 and L32 (in white) indicated the different lines of *sfh5 sfh7* seedlings with complemented *AtSFH7* expression. (Scale bar, 1 cm.) (B) Amount of chlorophyll a and b (mg/g fresh weight) in rosette leaves of 23-d-old Col-0, *sfh5*, *sfh7*, *sfh5 sfh7* and *sfh5 sfh7* seedlings with complemented *AtSFH7* expression, which was shown in light purple, dark red, light yellow, red, light green and dark green colors, respectively. Measurements were biologically repeated for three times. Data are mean \pm SEM, and statistical significance was determined by Student's *t* test ($*P < 0.05$). (C) Abnormal chloroplast development and altered thylakoid ultrastructure of *sfh5 sfh7*. Seventh rosette leaves of 23-d-old Col-0, *sfh5 sfh7* and *sfh5 sfh7* seedlings with complemented *AtSFH7* expression were observed using TEM. "S" and "T" (in red) denote starch granules and thylakoid, respectively. Red frame regions were enlarged. Scale bars, 10 μ m (1 to 3), 2 μ m (4 to 6), and 500 nm (7 to 9).

when NBD-PA was bound (and extracted) by Sec14 proteins. Indeed, addition of AtSFH5-Sec14 led to a dramatic increase in NBD-PA fluorescence, while human and yeast homologues presented little effect (Fig. 2E). However, little fluorescence changes were detected in the liposome-based phosphatidylinositol phosphate (PIP)-binding assays, suggesting that PIPs might not be the physiological ligands for Sec14 family (SI Appendix, Fig. S4C).

To assess the PA transfer ability, we carried out transport assays with donor liposomes (PC/PE) supplemented with NBD-PA (18:1/12:0 or 16:0/12:0) and acceptor liposomes (only PC/PE) (Fig. 2F and SI Appendix, Fig. S4D). Adding of AtSFH5-Sec14 resulted in the dequenching of NBD-PA signal, demonstrating

that AtSFH5 could efficiently transport PA between membranes. Notably, the transfer of 18:1/12:0 NBD-PA was faster than that of 16:0/12:0 NBD-PA, corroborating that the AtSFH5-Sec14 domain prefers PA with unsaturated and/or long acyl chain, exactly the major PA species synthesized in *Arabidopsis* ER (1). These in vitro results indicated that AtSFH5, but not yeast or human Sec14 proteins, specifically recognized PA embedded in liposomes, and efficiently transported PA between membranes.

Overall Structures of AtSFH5-Sec14 in Complex with PA. To investigate the mechanism of PA recognition, we tried to crystallize and determine the structures of AtSFH5-Sec14 in complex with

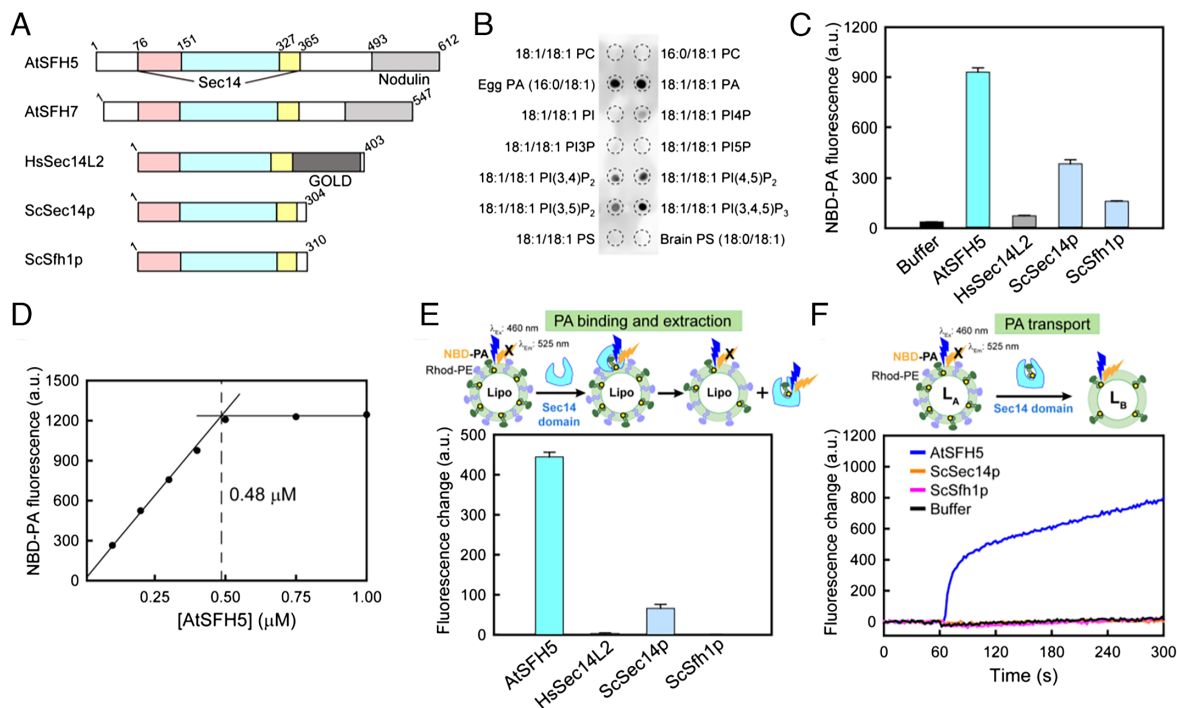


Fig. 2. AtSFH5 specifically transfers PA. (A) Schematic diagram of Sec14-like proteins from *Arabidopsis*, yeast and human. Structural regions are colored as follows: Sec14 domain (N-terminal subdomain, pink; core region, pale blue; C-terminal tail, yellow), nodulin domain (gray), GOLD domain (dark gray). (B) Protein-lipid overlay assay for AtSFH5-Sec14. Nitrocellulose membranes spotted with indicated phospholipids were overlaid with AtSFH5-Sec14 (80 μM), and bound proteins were detected by immunoblotting with anti-His antibody. (C) NBD-labeled lipid-binding assays with 18:1/12:0 NBD-PA. The contribution of buffer or methanol was subtracted from NBD signal. Proteins (final concentration of 0.4 μM) were added to a solution containing NBD-labeled lipid (2 μM), and NBD emission spectra at 525 nm were recorded ($\lambda_{ex} = 460$ nm). Experiments were biologically repeated three times, and data are mean \pm SEM (n = 3). (D) Fluorescence titration assay for NBD-PA binding to AtSFH5-Sec14. Protein aliquots were added to a solution containing 18:1/12:0 NBD-PA (2 μM). NBD emission spectra at 525 nm were recorded ($\lambda_{ex} = 460$ nm). (E) Liposome-based PA binding/extraction assay for AtSFH5, human Sec14L2 and yeast Sec14p or Sfh1p proteins. Proteins (final concentration of 0.5 μM) were added to liposomes (dioleoylphosphatidylcholine (DOPC)/dioleoylphosphatidylethanolamine (DOPE)/18:1/12:0 NBD-PA (green)/Rhod-PE (light purple) = 62.7/31.3/4/2 mol%, 50 μM lipids in total), and NBD signal was recorded ($\lambda_{ex} = 460$ nm) after 5 min. Experiments were biologically repeated three times, and data are mean \pm SEM (n = 3). (F) Liposome-based PA transport assays for AtSFH5-Sec14. Donor liposomes (DOPC/DOPE/18:1/12:0 NBD-PA (green)/Rhod-PE (light purple) = 62.7/31.3/4/2 mol%, 50 μM total lipids) were mixed with acceptor liposomes (DOPC/DOPE = 2/1 mol%, 50 μM total lipids). Proteins (0.5 μM) were added and NBD signal was recorded. Experiments were biologically repeated three times, and data are mean \pm SEM (n = 3).

L- α -PA and DPPA at resolutions of 1.95 Å and 2.1 Å, respectively (Fig. 3 A and B and *SI Appendix*, Table S1). Both structures comprised two molecules per asymmetric unit (referred to as Mol A and Mol B), and each molecule bound one PA (*SI Appendix*, Fig. S5 A and B). In the complex structures, the AtSFH5-Sec14 domain adopted typical two-lobed Sec14 fold. The N-terminal subdomain (residues 76 to 151) contained a tripod motif of helices α 1-3, and the C-terminal subdomain could be divided into two parts, a core region (152 to 326) and a C-terminal tail (327 to 365). The core region consisted of a five-stranded β -sheet (β 1-5) surrounded by helices α 4-10, with the PA ligand buried in a large pocket. The N-terminal subdomain sat on the top of ligand-binding pocket, while the C-terminal tail exhibited an extended conformation packing against the surface of core region and tripod motif. The last helix in Mol B was disordered in both structures, and structural analyses hereafter were on the basis of Mol A at 1.95 Å if not indicated.

The conformations of core region and N-terminal subdomain (if present), as well as their corresponding position and orientation, were highly conserved in plant, yeast, and human Sec14 structures (Fig. 3 A and B and *SI Appendix*, Fig. S5C) (22). Interestingly, the C-terminal tails adopted distinct conformations. In AtSFH5-Sec14, the N-terminal half of the C-terminal tail was a flexible loop shielding the core β -sheet; in particular, Pro340 and Trp341 made hydrophobic contacts with residues on strands β 1-2 and helix α 6 (Fig. 3C). The core helix α 6 also interacted with the C-terminal helix α 11 and its flanking loop, forming a hydrophobic groove to accommodate Leu77 and Ile79 from the

N-terminal subdomain. In addition, the charged or polar side chains of Arg358, His359 and Asn360 from the most C-terminal helix α 12 formed multiple hydrogen bonds with residues in the N-terminal tripod motif, directly or water-mediated (Fig. 3D). The massive hydrophobic and hydrophilic interactions likely stabilized the extended conformation of the C-terminal tail of AtSFH5-Sec14. However, even in the highly conserved yeast proteins, the presence of an additional, most N-terminal helix prevented the protrusion of the C-terminal tail toward the tripod motif.

To assess the role of the tail region, we generated step-wise C-terminal truncations and site-specific mutations on SFH5-Sec14; however, many mutations affected protein folding and solubility (Fig. 3E). In particular, two truncations removing the portion shielding the central β -sheet (Δ 327 to 365 and Δ 342 to 365), as well as substituting the key interacting residues (P340A/W341A), both led to fully insolubility. Deletion of the C-terminal one or two helices (Δ 353 to 365 and Δ 346 to 365) and mutations within this region reduced solubility of AtSFH5-Sec14, likely owing to disrupt interactions with the N-terminal subdomain. We also made some N-terminal truncations and mutations (Fig. 3E). Indeed, removing or mutation of the most N-terminal loop also impaired the solubility of recombinant proteins, while those of the tripod motif resulted in more severe effects. The soluble mutant proteins were subjected to the PA binding and transfer assays, and the activities were largely consistent with their solubility (Fig. 3E). Therefore, both the N-terminal subdomain and the C-terminal tail are required for the proper folding of the AtSFH5-Sec14 domain, but not directly involve in the PA transport.

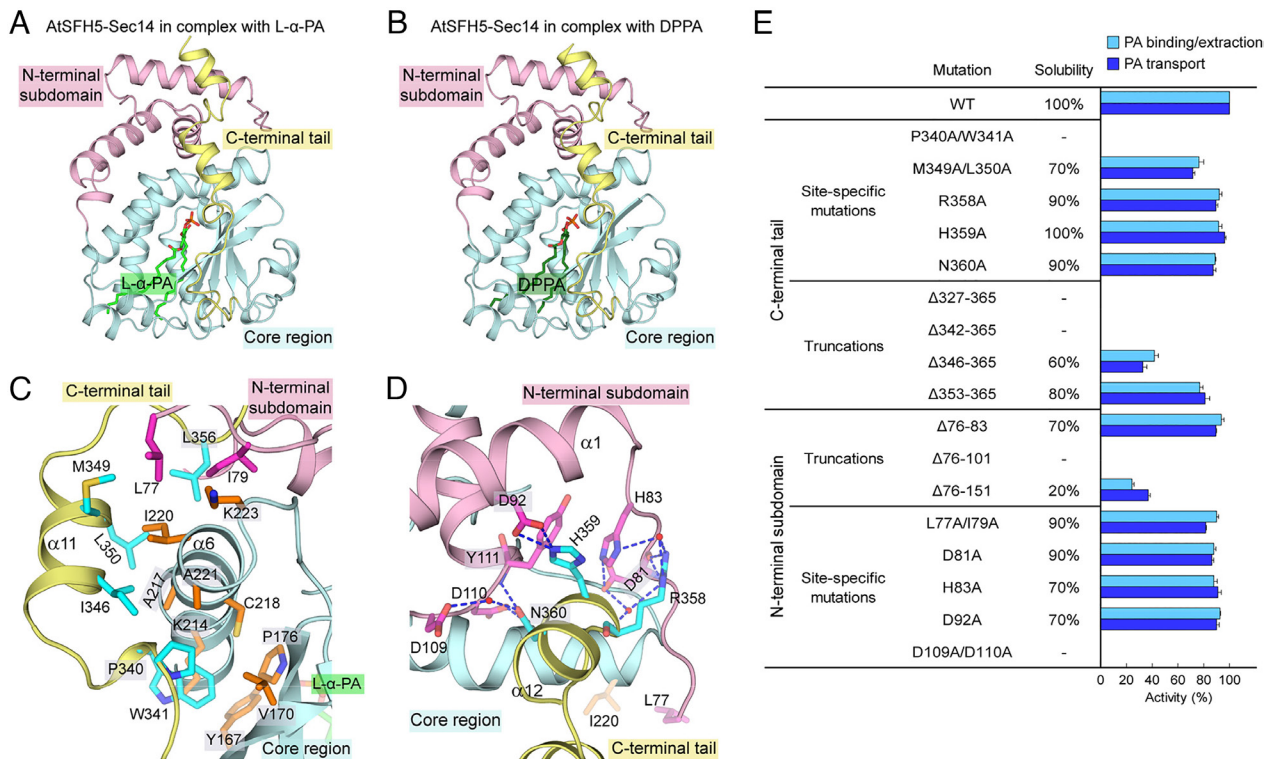


Fig. 3. Structures of PA-bound AtSFH5-Sec14. (A and B) Overall structures of AtSFH5-Sec14 in complex with L- α -PA (A) and DPPA (B). The color scheme follows as N-terminal subdomain with pink, core region with pale blue, C-terminal tail with yellow, and PA ligands are highlighted as green and forest sticks. (C and D) Close-up views of interactions mediated by C-terminal tail. The interacting residues of C-terminal tail are highlighted as cyan sticks, and those from the core region and N-terminal subdomain are shown as orange and magenta sticks, respectively. Blue dashed lines represent the polar interactions. (E) Solubility and activity of AtSFH5-Sec14 variants with mutations of C-terminal tail or N-terminal subdomain. Various variants were expressed in *Escherichia coli*, and soluble proteins were purified to homogeneity. The liposome-based PA binding/extraction and transfer assays were performed as Fig. 2 E and F. ND, not detected.

PA Recognition by AtSFH5-Sec14. In AtSFH5-PA complexes, the omit maps revealed the continuous electron density in the core, allowing the fitting of 16:0/18:1 PA (dominant species in L- α -PA mixture) and 16:0/16:0 DPPA, respectively (SI Appendix, Fig. S6 A and B). Both PA ligands nestled in the large cavity formed by central β -sheet and several α -helices. In AtSFH5-L- α -PA complex, the *sn*-1 chain (palmitoyl 16:0) made massive contacts with hydrophobic side chains from helices α 4-7 and flanking loops, while the *sn*-2 chain (oleoyl 18:1) lied in a hydrophobic groove formed mainly by residues on strands β 3-5 and helix α 8 (Fig. 4A). In addition, the phosphate moiety of PA interacted with Tyr167, Ser229, Thr231 from β -sheet and Asp258, Thr265 at C terminus of helix α 7, and the glycerol backbone was involved in direct and water-mediated hydrogen bonds as well. In AtSFH5-DPPA complex structure, the binding mode of the head group was largely conserved; however, locations of two acyl chains were switched compared with that in the L- α -PA complex (SI Appendix, Fig. S6C). The gate region of helices α 8-9 was implicated in modulating lipid access, which displayed a closed conformation in ScSfh1p and an open conformation in ScSec14p (20, 23). AtSFH5-Sec14 adopted the featured closed conformation, whose gate region interacted with one acyl chain to stabilize PA configuration in both AtSFH5-PA complexes. Considering that the AtSFH5-Sec14 domain could accommodate PA in different configurations, we hypothesized that PA might enter the lipid binding pocket of AtSFH5 in different orientations.

Sequence alignment revealed that PA-interacting residues were highly conserved in the Sec14 domain of AtSFH7, as well as in other SFH proteins (Fig. 4B and SI Appendix, Fig. S7). Based on the functional redundancy, it was believed that AtSFH7 could also transfer PA, and that PA could be the common ligand of

Arabidopsis SFH subfamily. However, residues involved in the recognition of PA glycerol backbone were varied in ScSec14p and ScSfh1p, which might account for the low activities for PA embedded in membranes (Fig. 2 E and F and SI Appendix, Fig. S4B). More strikingly, most of the polar or charged residues accommodating the PA head group in AtSFH5-Sec14 were substituted by hydrophobic amino acids in the HsSec14L2-Sec14 domain, and one of the acyl chain-binding groove was obstructed by bulky side chains of Trp164 and Tyr171. Consequently, HsSec14L2 only bound small ligands, but not phospholipids (Fig. 2C and SI Appendix, Fig. S4A). Therefore, plant SFH proteins, but not yeast and human homologues, can specifically recognize and transfer PA, even though their Sec14 domains are highly conserved in sequence and structure.

To confirm the PA binding mode, we generated a series of point mutations on AtSFH5-Sec14, and substitution of some key residues again resulted in markedly reduced protein solubility (Fig. 4C). The double-mutant L233W/I251W, engineered to sterically obstruct the binding of acyl chains, was completely insoluble, and the partially soluble individual substitutions both exhibited significantly decreased PA binding and transfer abilities. However, individually mutating Tyr167 and Ser229 to a bulky residue (Y167W and S229W), designed to impair the polar contacts with PA phosphate moiety, resulted in comparable protein solubility and PA binding/transfer activities to wild-type AtSFH5-Sec14. It has been reported that ScSec14p with double mutation of S173A/T175A exhibited marked decrease in PC transfer activity owing to the impaired PC headgroup binding pocket (20). However, PA binding and transfer by the cognate AtSFH5 mutant S229A/T231A were almost the same as that by the wild-type protein, corroborating that the PA binding mode of AtSFH5 was different from the PC

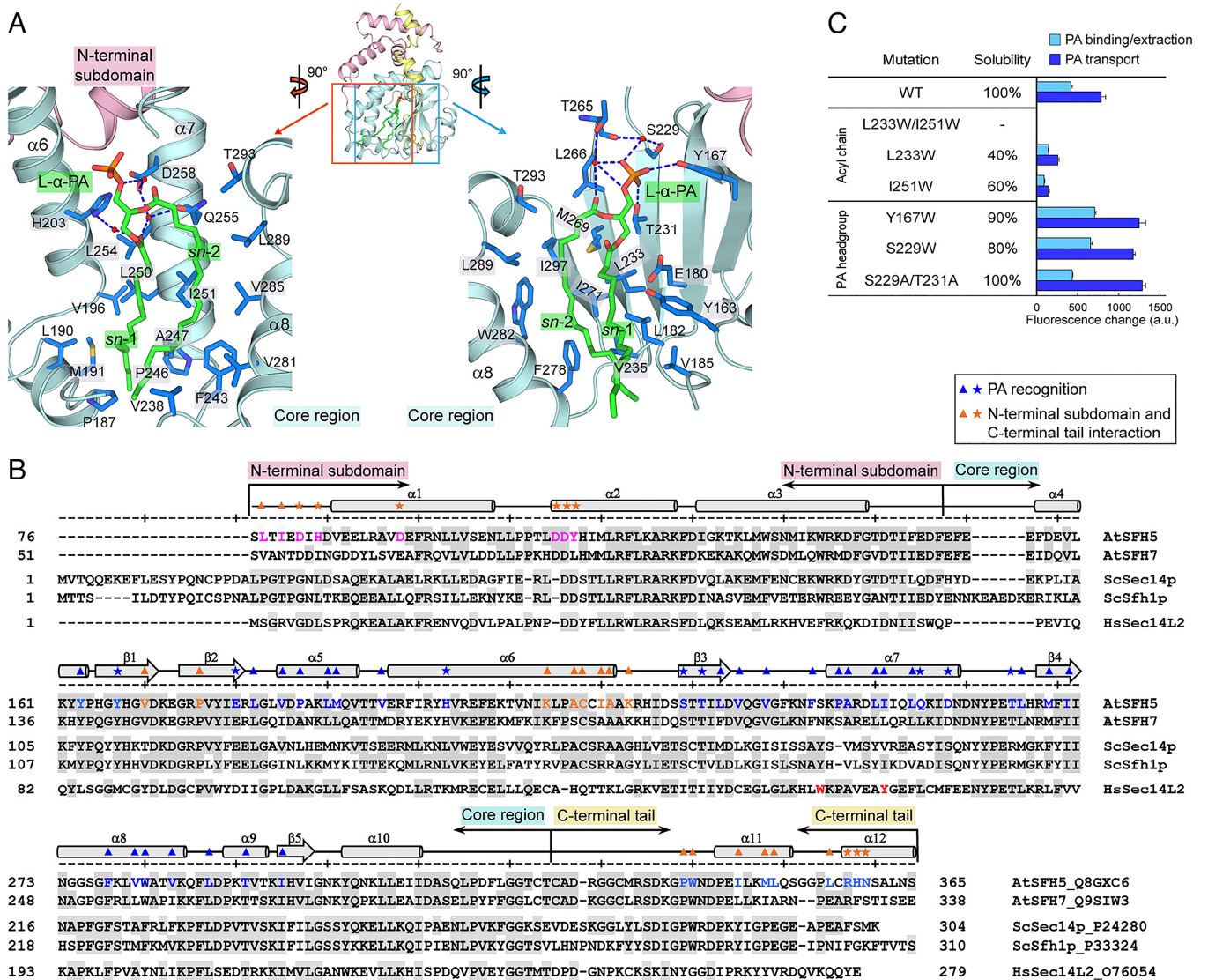


Fig. 4. Binding mode of L- α -PA to AtSFH5-Sec14. (A) Hydrophobic and hydrophilic interactions with L- α -PA. For clarity, part of the AtSFH5-Sec14 structure has been removed to show the PA binding pocket. Structural elements are colored as in Figure 3A and 3B. Residues of AtSFH5-Sec14 involved in recognition of PA are shown as blue sticks. Dashed line, polar interaction. (B) Structure-based sequence alignment of Sec14 domains from *Arabidopsis* (AtSFH5, AtSFH7), yeast (ScSec14p, ScSfh1p), and human (HsSec14L2) (corresponding UniProt IDs were shown). Residues of AtSFH5-Sec14 involved in recognition of PA are indicated by blue asterisks/triangles, and interacting residues at N-terminal subdomain and C-terminal tail are indicated by orange asterisks/triangles. (C) Solubility and activity of variants with mutated PA binding site of AtSFH5-Sec14. The liposome-based PA binding/extraction and transfer assays were performed as Fig. 2 E and F. Experiments were biologically repeated for three times, and data are mean \pm SEM ($n = 3$).

binding mode of ScSec14p. One plausible explanation for the non-affecting mutations was that the PA headgroup could still be stably bound by interacting with polar or charged residues from helix $\alpha 7$ (Fig. 4A). Together, our biochemical and structural analysis demonstrated that the core region of the Sec14 domain played a key role in AtSFH5 function as a PA transfer protein.

AtSFH5 and AtSFH7 Localize at ER and Chloroplast. Fusion proteins AtSFH5-yellow fluorescent protein (AtSFH5-YFP) [AtSFH5-red fluorescent protein (AtSFH5-RFP)] or AtSFH7-YFP (AtSFH7-RFP) were transiently expressed in tobacco (*Nicotiana benthamiana*) leaves or stably expressed in *Arabidopsis* protoplasts together with ER-rk CD3-959 (an ER marker) fused with mCherry or G-gk CD3-963 (a Golgi marker) fused with green fluorescent protein (GFP) (24) to determine their subcellular localization. Observations showed that both AtSFH5 and AtSFH7 were localized primarily in membrane structures (SI Appendix, Fig. S8A). Detailed analysis further showed that

ER-rk CD3-959-mCherry fully colocalized with AtSFH5-YFP and partially with AtSFH7-YFP (Fig. 5A), demonstrating AtSFH5 and AtSFH7 localize at ER. However, AtSFH5-RFP or AtSFH7-RFP did not show colocalization with G-gk CD3-963-GFP (SI Appendix, Fig. S8B), indicating they do not localize at Golgi apparatus, and the PA transfer by them did not depend on the vesicle secretory pathway from Golgi. Further observations showed that AtSFH5-YFP and AtSFH7-YFP also localized in chloroplasts (Fig. 5B), indicating the double localization of AtSFH5 and AtSFH7 in ER and chloroplasts.

Most of *Arabidopsis* SFH proteins contain a plant-specific nodulin domain at C-terminal to the Sec14 domain, connected by a long flexible region (~100 residues). Considering that the nodulin domain was crucial for subcellular localization of SFH proteins (25), our analysis indeed showed that deletion of the nodulin domain of AtSFH5 and AtSFH7 resulted in the obviously altered subcellular localization in membrane structures. However, there was no obvious change of AtSFH5 and AtSFH7 subcellular

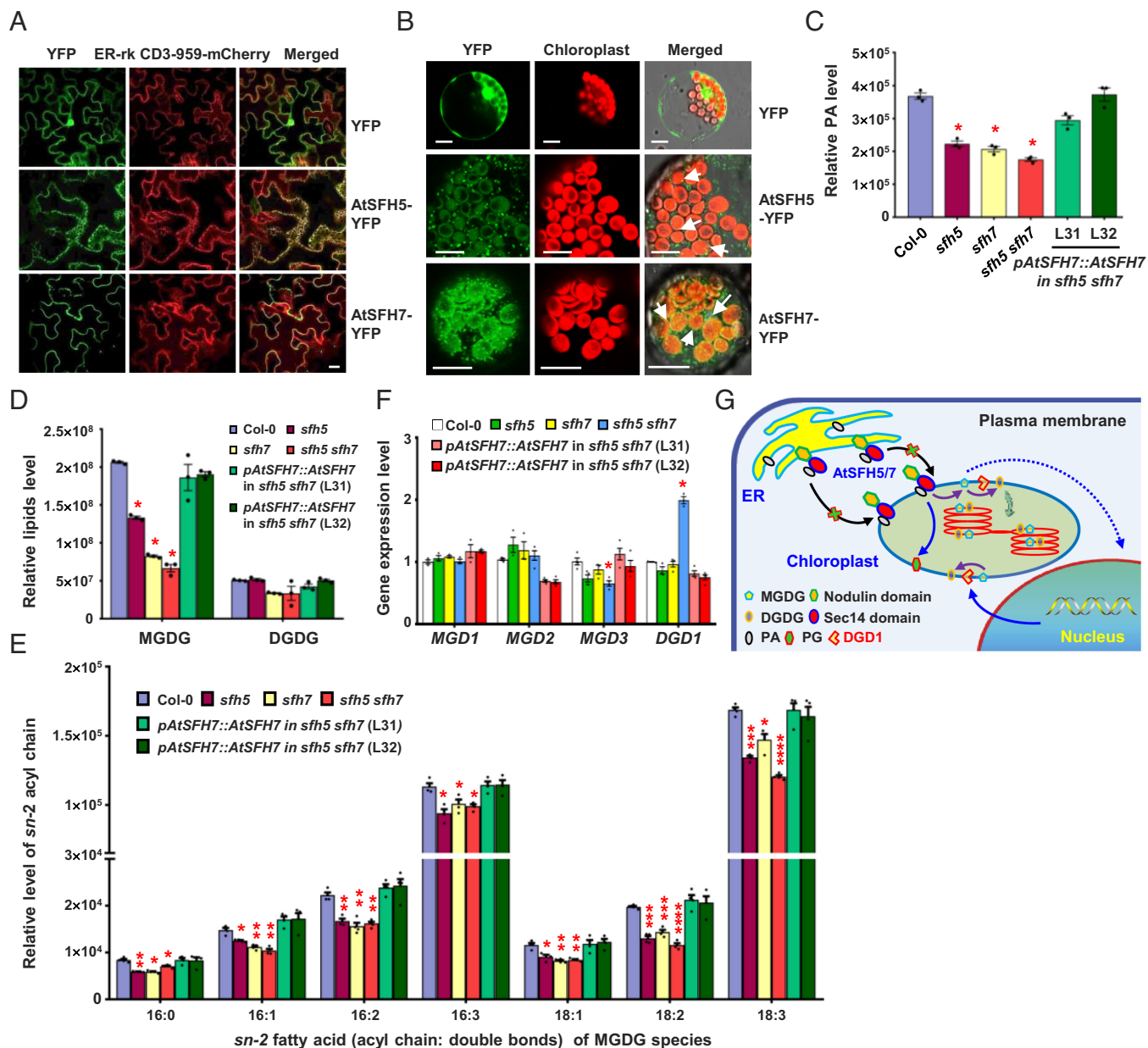


Fig. 5. AtSFH5/AtSFH7-mediated PA transfer regulates lipid synthesis of chloroplast. (A) Subcellular localization studies by transiently expressing fusion proteins in *N. benthamiana* epidermal cells showed that AtSFH5-YFP and AtSFH7-YFP colocalize with ER-rk CD3-959-mCherry (an ER marker). (Scale bar, 20 μ m.) (B) Observation of *Arabidopsis* mesophyll protoplasts transiently expressing fusion proteins showed that AtSFH5-YFP and AtSFH7-YFP localize at membrane of chloroplasts (highlighted by arrows). (Scale bars, 10 μ m.) (C) Quantitative analysis of PA level of isolated chloroplasts from rosette leaves of 23-d-old Col-0, *sfh5*, *sfh7*, *sfh5 sfh7* and *sfh5 sfh7* seedlings with complemented AtSFH7 expression. Relative PA levels are shown by peak intensity of electrospray ionization mass spectrometry/mass spectrometry (ESI-MS/MS). Data are mean \pm SEM (n = 3), and statistical significance was determined by Student's *t* test (**P* < 0.05). (D) Quantitative analysis of MGDG and DGDG levels of isolated chloroplasts from rosette leaves of 23-d-old Col-0, *sfh5*, *sfh7*, *sfh5 sfh7* and *sfh5 sfh7* seedlings with complemented AtSFH7 expression, which were shown in light purple, dark red, light yellow, red, light green and dark green colors, respectively. Relative MGDG or DGDG levels are shown by peak intensity of ESI-MS/MS. Data are presented as mean \pm SEM (n = 3), and statistical significance was determined by Student's *t* test (**P* < 0.05). MGDG, monogalactosyldiacylglycerol. DGDG, digalactosyldiacylglycerol. (E) Quantitative analysis of fatty acid composition at the *sn*-2 position of the glycerol backbone of chloroplast MGDG. The rosette leaves of 23-d-old Col-0, *sfh5*, *sfh7*, *sfh5 sfh7* and *sfh5 sfh7* seedlings with complemented AtSFH7 expression were analyzed. Relative levels of fatty acid at the *sn*-2 position are shown by peak intensity of EIEIO-MS. Fatty acids are indicated with the number of carbons: number of double bonds. Data are mean \pm SEM (n = 4), and statistical significance was determined by Student's *t* test (**P* < 0.05; ***P* < 0.001; ****P* < 0.0001; *****P* < 0.00001). EIEIO-MS, electron impact excitation of ions from organics mass spectrometry. (F) qPCR analysis showed the increased expression of *DGD1* under deficiency of AtSFH5 and AtSFH7. Seedlings of Col-0, *sfh5*, *sfh7*, *sfh5 sfh7* and *sfh5 sfh7* with complemented AtSFH7 expression were grown in dark for 7 d, then transferred to light for 4 h. *ACTIN7* gene was used as an internal reference, and relative expression of examined genes in Col-0 is defined as "1." Experiments were repeated three times, values are mean \pm SEM, and statistical significance was determined by Student's *t* test (**P* < 0.05). (G) A hypothetical model illustrating the crucial roles of AtSFH5/AtSFH7-mediated ER-to-chloroplast PA transfer in regulating chloroplast lipid synthesis and thylakoid development. AtSFH5 and AtSFH7 localize at both ER and chloroplast, bind, and transfer PA from ER to chloroplast, to ensure the proper lipid synthesis and assembly of chloroplast or thylakoid membrane components. Decreased chloroplast PA content under deficiencies of AtSFH5 and AtSFH7 resulted in the significantly reduced level of PG and MGDG, and hence the abnormal thylakoid development. Reduced MGDG might lead to the up-regulated expression of *DGD1* gene to maintain the DGDG level through retrograde signaling.

localization with deletion of the Sec14 domain (SI Appendix, Fig. S9), indicating that the Sec14 domain was not involved in the subcellular localization determination of SFH proteins.

Lipid Metabolism Is Significantly Altered in *sfh5 sfh7* Chloroplasts. To further investigate the effects of AtSFH5 and AtSFH7 through transporting PA and hence chloroplast development, lipid

constituent of chloroplasts was analyzed by innovatively applying lipidomic approach of chloroplast organelles. Chloroplasts were isolated from 23-d-old plants and verified to be intact, and lipids were then extracted and quantified using ESI-MS/MS. Results showed that the phospholipids were reduced, particularly PA was significantly decreased in *sfh5 sfh7* chloroplasts (Fig. 5C). Detailed analysis showed that species of PA with long unsaturated fatty acyl chains (total carbon:double bond; 34:2, 34:3, 36:1, 36:2, 36:4, 36:5, 36:6) were significantly decreased in *sfh5 sfh7* (SI Appendix, Fig. S10A), which corroborated that AtSFH5 preferred to transport PA with long and unsaturated acyl chains (Fig. 2F and SI Appendix, Fig. S4D). Phospholipids PC and PG of chloroplasts were also decreased in *sfh5 sfh7* (SI Appendix, Fig. S10B). Combined with the results that AtSFH5-Sec14 had the transfer activity of PC (SI Appendix, Fig. S4A), which suggested that AtSFH5 and AtSFH7 might also transport PC to outer envelope membranes of chloroplasts. PA necessitated the PG synthesis in thylakoid membrane of chloroplasts (26), and decreased supply of precursor PA might impair the synthesis of chloroplast-derived PG.

Lipid profiling analysis also showed the significantly decreased amount of galactoglycerol lipid, MGDG in *sfh5 sfh7* chloroplasts (Fig. 5D). PA phosphatase was exclusively associated with the inner envelope membranes of chloroplasts and dephosphorylates PA into DAG, which was further synthesized into MGDG by MGDG synthase (MGD) (27). Decreased MGDG level indicated the involvement of AtSFH5 and AtSFH7 in the regulation of homeostasis of chloroplast lipids through transporting PA to chloroplast and importance of them for successive MGDG synthesis.

In plant cells, the prokaryotic pathway in the chloroplast produced glycerolipids with a C16 fatty acyl moiety at the *sn*-2 position, whereas the eukaryotic pathway generated glycerolipid molecules with only C18 fatty acids at *sn*-2 (28). To further confirm the PA transfer from ER to chloroplast in vivo by AtSFH5 and AtSFH7, we analyzed the C18 fatty acyl moiety at the *sn*-2 position of MGDG in *sfh5 sfh7*. Using the approach of electron impact excitation of ions from organics mass spectrometry (EIEIO-MS), we first identified the fatty acyl chain at *sn*-1 position in MGDG through acyl diagnostic peaks of cleavage site (SI Appendix, Table S2) and illustrated the cleaved peaks of 18:2 or 18:3 at *sn*-1 from the bond of O-(C1=O), C1-O and C1-C2 in MGDG, respectively (SI Appendix, Fig. S11), then the fatty acids at *sn*-2 in MGDG was deduced from its parent ion and *sn*-1 fragment (relative levels were quantitated based on the peak intensity of fragments). Based on the level of C18 and C16 fatty acyl chains within each MGDG (SI Appendix, Fig. S12), analysis of the total C16 and C18 compositions showed that the total C18 fatty acids at the *sn*-2 were significantly decreased ($P < 0.001$), and 18:2 and 18:3 were with lower level ($P < 0.00001$) in *sfh5 sfh7* than those in single-mutant *sfh5*, *sfh7*, or Col. The decreased level of C18 fatty acids at the *sn*-2 was more significant than that of C16 fatty acids at the *sn*-2 in *sfh5 sfh7* (Fig. 5E), indicating a disrupted ER-to-plastid (chloroplast) lipid transfer in *sfh5 sfh7*. In addition, the distribution of total fatty acid composition was consistent with previous studies (4–7), indicating that EIEIO-MS was a useful approach for regioisomeric identification of MGDG in plants.

MGDG is further synthesized as DGDG to involve in chloroplast development and environmental response, and the MGDG:DGDG ratio is critical for chloroplast shape (29). Analysis showed the unaltered DGDG level in *sfh5 sfh7* chloroplasts (Fig. 5D), which led to a decreased MGDG:DGDG ratio that may affect the chloroplast development. Based on that PA and/or PG are necessary for the activation of *MGD1–MGD3* and

in vitro supply of PA and/or PG promotes the expression of *MGD1* (30), analysis of transcription levels showed that expressions of *MGD1–MGD3* genes were unaltered, while that of *DGD1*, the major chloroplast DGDG synthase through converting MGDG and uridine diphosphate galactose (UDP)-galactose into DGDG (31), was obviously increased (Fig. 5F). Considering that *DGD1* is nucleus-encoding gene, it is suggested that reduced MGDG level in chloroplast may retrograde promote the *DGD1* expression, leading to the unaltered DGDG level under deficiency of *AtSFH5* and *AtSFH7*.

By determining the structures of AtSFH5-Sec14 in complex with PA ligands, our studies elucidated the structural basis for binding and transferring characteristics of SFH proteins, and revealed the molecular mechanisms of PA-ligand specificity among different Sec14 proteins. AtSFH5 and AtSFH7 transport PA from ER to chloroplast, to maintain the proper assembly of chloroplast and thylakoid membrane components (Fig. 5G). Reduced PA from ER to chloroplast results in the altered lipid homeostasis (significantly decreased level of PA and MGDG), and hence the defective development and functions of chloroplast and thylakoid, demonstrating the significance of ER-chloroplast PA transfer and lipid trafficking in buildup of chloroplasts.

Discussion

As the central metabolite of glycerolipid biosynthesis, PA transport necessitates the synthesis of glycerolipids or galactoglycerolipids. Human Sec14-containing proteins can transport a number of hydrophobic ligands, while yeast ScSec14p recognizes phospholipids PC and PI in vivo (14, 32). In model plant *Arabidopsis*, AtSFH1 exhibits intrinsic PI/PC binding activity and chloroplast-localized Sec14-like protein (CPSFL1) (also referred to as AtPITP7) preferentially binds to PI monophosphates and PA (2). The Sec14 domains are highly conserved and how Sec14 proteins precisely recognize distinct phospholipids and other hydrophobic ligands remains unknown, and extensive structural studies will help to understand the molecular mechanisms of ligand specificity. Our studies demonstrated that AtSFH5 strongly and specifically bind to and transfer PA between membranes. A largely conserved ligand-binding pocket of Sec14 domains from *Arabidopsis*, yeast and human accommodates various ligands. The PA head group situates in binding cavity of AtSFH5-Sec14, which is similar to the PC/PE binding mode of yeast ScSfh1p, but very different from the PI binding mode with the inositol headgroup nestled between core region and N-terminal tripod motif. The nonconservation of polar or charged residues involved in recognition of the PA head group (Fig. 4B and SI Appendix, Fig. S7) provide plausible explanation why yeast and human members cannot efficiently recognize and transfer PA embedded in membranes. However, residues involved in recognition of PC, PE, and PI from ScSfh1p are also conserved in AtSFH5, indicating that AtSFH5 might bind these phospholipids, which is consistent with that AtSFH5-Sec14 can bind NBD-PC (SI Appendix, Fig. S4A). In addition, binding/trafficking of other ligands by plant SFH proteins could not be excluded. These results shed light on understanding the recognition mechanism of lipid-binding proteins and interorganelle lipid transport of cells, and provide informative hints to investigate their roles in regulating lipid metabolism and plant development.

A number of human and plant Sec14 members are modular proteins with various functional domains in addition to the conserved Sec14 domain. In the reported structures, human HsSec14L2/3/4 and neurofibromin (NF1) contain a GOLD domain or a PH domain following the Sec14 domain, respectively (33). These additional domains bind at the bottom of the Sec14

domain, opposite to the tripod motif (*SI Appendix, Fig. S5C*). Consequently, the C-terminal tail of human Sec14 domains are relatively short and oriented differently from that in AtSFH5-Sec14, which first uncovered the nature why the plant Sec14 domain of SFH could specifically bind PA. In addition, the plant-specific nodulin domain of *Arabidopsis* SFH proteins is necessary for whose proper subcellular localization, and it is interesting to explore the structure of the plant-specific nodulin domain, and whether and how the nodulin domain regulates the function of the Sec14 domain.

Biosynthesis of chloroplast membrane lipids in seed plants involves two organelles and three membrane bilayers: ER, chloroplast inner and outer envelope membranes. The membrane contact sites (MCSs) and tethering proteins associated interorganelle communication between ER and other organelles have been extensively characterized in mammal and yeast (34). Recent study revealed the dynamic structures of ER-chloroplast MCSs in plant cells (35), which make the close proximity (usually 10 to 40 nm in distance) enabling the PA transfer from ER to chloroplast. Previously identified TGD complex involves in PA transfer from ER to plastids (4–7), and NDGD1 binds PA and mediates the PA-dependent membrane fusion in vitro (18); our results identify a PA transport mechanism that PA is transferred from ER by AtSFH5 and SFH7 for establishing the specialized thylakoid membrane of chloroplast, providing clues on regulation and effects of interorganelle phospholipids trafficking. Whether PA trafficking from ER to chloroplast happened on ER-chloroplast MCSs remained to be studied.

Systemic analysis of organelle lipid compositions helps to elucidate the development and functions of various organelles. In animals, lipidomic analysis of organelles uncovered the lipids coordinated the diurnal rhythmicity in intracellular organelles (nucleus and mitochondria) in mouse liver cells (36). Composition of chloroplast galactolipids was analyzed by thin layer chromatography, mixed DAGs are separated by chiral chromatography, and the acyls are analyzed by gas chromatography mass spectrometry (GC-MS) previously (4). In this study, analysis of chloroplast lipidome was innovatively developed, allowing the comprehensive analysis of chloroplast lipid species and classes. Deficiency of AtSFH5 and AtSFH7 caused the decreased PA species with long unsaturated fatty acid chains in chloroplasts (*SI Appendix, Fig. S10A*), the majorly synthesized PA in *Arabidopsis* ER (1), which is consistent with the faster transfer of 18:1/12:0 NBD-PA, compared with 16:0/12:0 NBD-PA, by AtSFH5-Sec14. Lipidomic analysis of chloroplast not only confirms that galactolipid MGDG and phospholipid PG are the major lipids in chloroplasts, but also quantifies the different species, providing informative clues on studying the role of lipids in chloroplast development.

Recently, the mass spectrometry-based methodologies have made great advances in molecular characterization of lipids. The well-documented method of EIEIO-MS was applied to distinguish regioisomers of lipidome, as well as a uniquely defined distribution of acyl chains within each lipid class, such as, *sn-1* and *sn-2* in phospholipids/ galactoglycerol lipid in porcine brain or *sn-2* and (*sn-1/ 3*) in triacylglycerols from natural lipids extract (olive oil), which represented the head group and regioisomeric assignment of identified acyl groups and carbon-carbon double bond locations within the acyl chains based on the energetic production of radical z^{\bullet} fragments with free electrons ~ 10 eV (37–39). By applying EIEIO-MS to analyze the C18 fatty acyl moiety at the *sn-2* position of MGDG in *sfh5 sfh7*, we demonstrated that the total C18 fatty acids at the *sn-2* were significantly decreased in *sfh5 sfh7*, providing evidence that AtSFH5 and AtSFH7 had the ability to transfer PA from ER to chloroplast in vivo.

Abnormal synthesis of galactolipids MGDG impaired the photosynthesis, chloroplast ultrastructure, and photosynthetic activity (3, 31). Decrease in MGDG caused the changed ratio of bilayer-to nonbilayer-forming membrane lipids, and an increased ratio of MGDG:DGDG resulted in the altered chloroplast shape (29). Significantly reduced MGDG and normal DGDG amounts led to the decreased ratio of MGDG:DGDG and altered chloroplast shape (smaller size with a flatter shape) in *sfh5 sfh7*, indicating the homeostasis of MGDG/DGDG is crucial for normal chloroplast development. Although MGDG level is significantly reduced, the up-regulated *DGD1* gene may lead to the normal level of DGDG in *sfh5 sfh7*, suggesting that altered MGDG level/lipid metabolism may regulate the expression of the nucleus-encoded *DGD1* gene through a retrograde signaling.

Materials and Methods

Plant Materials and Growth Conditions. Seeds of *A. thaliana* Col-0, various mutants, and transgenic lines were surface sterilized, then sown on plates containing 1/2 Murashige and Skoog (MS) medium (Duchefa Biochemie) and stratified at 4 °C for 48 h in the dark before germination. *A. thaliana* and tobacco (*Nicotiana benthamiana*) plants were grown in phytotron at 22 °C under 16-h light/8-h dark photoperiod.

Identification of Mutants and Generation of Double Mutants. Genomic sequences of AtSFH5 (At1g75370) and AtSFH7 (At2g16380) were used to query flanking sequence database of the T-DNA insertion database of Salk Institute (<http://signal.salk.edu/cgi-bin/tdnaexpress>). Mutants *sfh5* (SALK_114805C) and *sfh7* (SALK_113006C) were obtained and a PCR-based approach was used to confirm the insertion of T-DNA and to identify homozygous lines.

To generate double mutants, *sfh7* was used as the pollen donors in crosses to *sfh5*. F₂ plants derived from the cross were screened for homozygous mutants. Primers are listed in *SI Appendix, Table S3*.

Constructs and Plant Transformation. Constructs pCambia1300-SFH-5pro-GUS, pCambia1300-SFH7pro-GUS and pCambia1300-SFH7pro-SFH7 were generated and introduced into *Agrobacterium tumefaciens* strain GV3101. Transformation of Col-0 or *sfh5 sfh7* double mutant (for complementation studies) was performed by floral dip method. Transgenic seeds were screened on 1/2 MS plates containing hygromycin. At least three independent transgenic lines were identified for each construct and analyzed.

Quantitative RT-PCR (qPCR) Analysis. qPCR analyses were performed to examine the transcription of AtSFH5 and AtSFH7 in various tissues, and transcription of genes *MGD1-3*, and *DGD1-2* in Col-0, *sfh5*, *sfh7*, *sfh5 sfh7*, and *sfh5 sfh7* with complemented AtSFH7 expression. Total RNAs were extracted from harvested samples with TRIzol reagent (Invitrogen) according to the manufacturer's manual. Reverse transcription was performed using the reverse transcription kits (Toyobo), and resultant single-strand cDNAs were used as templates for qPCR using a SYBR Green qPCR kit (real-time PCR Master Mix; Toyobo) with a Rotor-Gene real-time thermocycler R3000 (Corbett Research). *ACTIN* gene (AT5G09810) was used as an internal control, and relative expression of examined genes was calculated using a comparative $\Delta\text{-}\Delta\text{Ct}$ method. Primers are listed in *SI Appendix, Table S2*.

GUS Staining Assays. GUS assay was performed as previously described (40) with few modifications. Tissues were placed directly into GUS reaction buffer (0.5 mg/mL X-glucuronic acid, 10 mM ethylene diamine tetraacetic acid (EDTA), 0.1% Triton X-100, and 2 mM potassium ferri/ferrocyanide in 50 mM phosphate buffer, pH 7.0) and incubated overnight at 37 °C after vacuumization for 20 min. Stained tissues were cleared in 70% ethanol and observed using differential interference contrast microscopy (Nikon SMZ1500).

Subcellular Localization Studies. Coding region of AtSFH5 was amplified and then subcloned into vector pA7 (C terminus fusion). Nucleotide sequences encoding CaMV35S promoter, AtSFH5, YFP and nopaline synthase (NOS) terminator were cloned into pCambia-1300 vector to generate pCambia-AtSFH5-YFP construct. A similar approach was used for AtSFH5-RFP, AtSFH7-YFP and AtSFH7-RFP fusion proteins, or deletion of nodulin (AtSFH5 Δ Nodulin-YFP, residual 1 to 327;

AtSFH7 Δ Nodulin-YFP, residual 1 to 301) or Sec14 domain (AtSFH5 Δ Sec14-YFP, residual 328 to 612; AtSFH7 Δ Sec14-YFP, residual 328 to 548). Resultant constructs were transformed into *A. tumefaciens* strain GV3101. Leaves of 3-wk-old tobacco plants were infiltrated, and fluorescence were observed after inoculation for 2 d (confocal laser scanning microscopy, Olympus FV1000).

Protein Preparation. AtSFH5-Sec14 domain (residues 76 to 365) and truncations (Δ 76 to 83/101/151, Δ 327/342/346/353 to 365) were cloned into pET21b vector with C-terminal His₆-tag. All site-specific mutations were generated by standard Quickchange procedure and verified by DNA sequencing. ScSec14p and ScSfh1p were also cloned into pET21b. The HsSec14L2-Sec14 domain (residues 1 to 275) was cloned into pET28b with N-terminal His₆-tag. ScOsh4p was cloned into pGEX-2T vector with N-terminal glutathione S-transferase (GST) tag. All proteins overexpressed in *Escherichia coli* BL21 (DE3) cells at 18 °C for 14 h upon induction with 200 μ M isopropyl β -D-1-thiogalactopyranoside (IPTG), were purified by Ni-NTA (QIAGEN) or GS4B (GE Healthcare) affinity chromatography columns and then by ion exchange and gel filtration chromatography (Source-15Q/15S and Superdex-200/75 increase, GE Healthcare) at 4 °C. The GST tag was cleaved by thrombin protease and removed through GS4B affinity chromatography columns. The purified proteins in a buffer containing 10 mM Tris-HCl, pH 8.0, 150 mM NaCl and 2 mM dithiothreitol (DTT) were stored at -80 °C. Protein concentrations were determined spectrophotometrically using theoretical molar extinction coefficients at 280 nm and subjected to biochemical analyses and crystallization experiments.

For NBD labeling of PH_{FAPP}, after removing DTT by gel filtration on Superdex-75 10/300 columns (GE Healthcare), the proteins were mixed with 10-fold molar excess of N, N'-dimethyl-N-(iodoacetyl)-N'-(7-nitrobenz-2-oxa-1,3-diazol-4-yl) ethylenediamine (N, N'-dimethyl-N-(iodoacetyl)-N'-(7-nitrobenz-2-oxa-1,3-diazol-4-yl) ethylenediamine (IANBD)-amide, Molecular Probes). After incubation at 4 °C overnight, the reaction was stopped by adding a 10-fold excess of L-cysteine over the probe. The free probe was removed by gel filtration chromatography and the NBD-labeled PH_{FAPP} was analyzed by sodium dodecyl sulfate-polyacrylamide gel electrophoresis (SDS-PAGE) and spectroscopy. The labeling yield ($\sim 100\%$) was estimated from the ratio of the optical density of PH_{FAPP} at 280 nm ($\epsilon = 29,450$ M⁻¹ cm⁻¹) and NBD at 495 nm ($\epsilon = 25,000$ M⁻¹ cm⁻¹).

Protein-Lipid Overlay Assay. Lipid dissolved in methanol/chloroform/water (2:1:0.8, v/v/v), and 500 pmol each of the lipids was then immobilized and air-dried on BioTrace NT Nitrocellulose Transfer Membrane (Pall Corporation). Membranes were blocked with 5% bovine serum albumin (BSA) in PBST (4 mM NaH₂PO₄, 16 mM Na₂HPO₄, 150 mM NaCl, 0.1% Tween-20) at room temperature for 1 h, and then incubated with 80 nM protein in blocking buffer at 4 °C for 6 h. The membrane was washed four times over 10 min in PBST. Bound proteins were detected by immunoblotting with anti-His antibody (1:1,000; YTHXbio, catalog no. ZA004) and then with horseradish peroxidase-conjugated anti-mouse secondary antibodies (1:5,000; Invitrogen, catalog no. 31430).

NBD-Labeled Lipid-Binding Assay. A suspension (496 μ L) containing 2 μ M NBD-labeled phospholipid (stock in methanol), was incubated at 25 °C under constant stirring in TSE buffer (20 mM Tris-HCl pH 7.5, 150 mM NaCl and 2 mM EDTA). After 1 min, protein (4 μ L) was injected to reach 0.4 μ M. This setting is to ensure the NBD signal is detectable and stable, and also can reflect the binding affinity differences among proteins. The mixture was incubated at 25 °C for 2 min, and then the NBD spectrum was recorded at 525 nm upon excitation at 460 nm. The increased NBD fluorescence mirrors the NBD-labeled lipid is bound by Sec14 proteins, because the NBD (7-nitrobenz-2-oxa-1,3-diazol-4-yl) group fluoresces strongly when buried in a hydrophobic environment (22).

Fluorescence Titration Assay. A suspension (490 μ L) containing 2 μ M 18:1/12:0 NBD-PA (stock in methanol), was incubated at 25 °C under constant stirring in TSE buffer. After 1 min, protein aliquots were injected. After each addition of protein, the mixture was incubated at 25 °C for 2 min, and then the NBD spectrum was recorded at 525 nm upon excitation at 460 nm.

Liposome Preparation. Lipids in chloroform were mixed at the desired molar ratio in vials; the solvent was removed using nitrogen gas yielding a lipid film on sides of a bottom flask. The lipid film was thoroughly dried to remove organic solvent by placing the vial on a vacuum desiccator overnight. Lipid films were hydrated in TSE buffer (20 mM Tris-HCl, pH 7.5, 150 mM NaCl and 2 mM EDTA) to obtain a suspension of elementary multilamellar liposomes. Multilamellar

liposome suspension was subjected to eight freeze-thaw cycles using liquid nitrogen and water bath followed by extrusion through polycarbonate filters of 0.2- μ m pore size using a mini-extruder (Avanti Polar Lipids). Liposomes were stored at 4 °C in dark and used within 2 d.

Liposome-Based PA Binding/Extraction Assay. The suspension (495 μ L) containing liposomes (DOPC/DOPE/Rhod-PE/NBD-PA = 62.7/31.3/2/4 mol%, 50 μ M total lipids) was incubated at 25 °C in a small quartz cuvette under continuous stirring in TSE buffer. After 1 min, protein (5 μ L) was injected to reach 0.5 μ M. NBD spectrum was recorded at 525 nm upon excitation at 460 nm before and 2 min after injection of proteins. The NBD fluorescence change mirrors NBD-PA is bound or further extracted from liposomes by Sec14 proteins. The intensity at 525 nm recorded 2 min after the addition of protein corresponds to F . A control signal (F_0) was measured in the absence of protein to subtract the contribution of liposomes or buffers. Fluorescence change is calculated by $F - F_0$.

Liposome-Based PIP Binding/Extraction Assay. PIP Binding/Extraction assay was performed as previously described with few modifications (41, 42). The sample (500 μ L) containing liposomes (DOPC/DOPE/PIP = 64/32/4 mol%, 100 μ M total lipids) was mixed with NBD-PH_{FAPP} (250 nM) at 25 °C in a small quartz cuvette under continuous stirring in TSE buffer. The NBD fluorescence spectrum was recorded at 525 nm upon excitation at 460 nm before and 2 min after injection of 2 μ M proteins corresponding to F_{\max} and F . Fluorescence change is calculated by $F_{\max} - F$.

Liposome-Based PA Transport Assay. PA transport assay was performed as described previously with few modifications (13). A suspension (495 μ L) of donor liposomes L_A (DOPC/DOPE/Rhod-PE/NBD-PA = 62.7/31.3/2/4 mol%, 50 μ M total lipids) and acceptor liposomes L_B (DOPC/DOPE = 2/1 mol%, 50 μ M total lipids) was incubated at 25 °C under constant stirring in TSE buffer. After 1 min, protein (5 μ L) was injected to reach 0.5 μ M. PA transport was followed by measuring the NBD signal at 525 nm upon excitation at 460 nm. The NBD fluorescence change mirrors the redistribution of NBD-PA between L_A and L_B liposomes. The fluorescence at 525 nm was increased upon addition of liposomes, which may be due to the spontaneous transfer of lipid. So, the contribution of liposome alone was subtracted from the NBD signal to reflect the pure contribution of protein.

Crystallography. DPPA, dioleoyl phosphatidic acid (DOPA), and L- α -PA was dissolved in chloroform (2 mg/mL in stock), and an aliquot was evaporated using nitrogen gas yielding a thin lipid film. Each ligand was mixed with the AtSFH5-Sec14 domain protein (80 μ M) at a 2:1 molar ratio, and mixtures were incubated at 25 °C for 2 h and then subjected to crystallization trials. Crystals were grown by the vapor-diffusion method in hanging-drop by mixing the protein-ligand complex (~ 3 mg/mL) with an equal volume of reservoir solution at 18 °C. Crystals of the AtSFH5-Sec14 domain-L- α -PA complex were obtained with reservoir buffer containing 0.1 M Bis-Tris propane, pH 6.5, 20% PEG3350, and 0.2 M NaNO₃. Crystals of the AtSFH5-Sec14 domain-DPPA complex were obtained with reservoir buffer containing 0.1 M MES, pH 6.0, 20% PEG6000, and 0.2 M NaCl. The crystals were equilibrated in a cryoprotectant buffer containing reservoir buffer supplemented with 20% ethylene glycol before snap-frozen in liquid nitrogen.

The diffraction data sets were collected at beamline 17U of Shanghai Synchrotron Radiation Facility (Shanghai, China) and in-house Rigaku XtaLAB. The diffraction datasets were processed with HKL2000. The AtSFH5-Sec14 domain-DPPA complex structure was solved by molecular replacement using Phaser with yeast ScSec14 structure (PDB code: 1AUA) as search model, and structure of the AtSFH5-Sec14 domain-L- α -PA complex was solved using the AtSFH5-Sec14 domain-DPPA complex as search model (43). Standard refinement was performed with Coot, PHENIX, and REFMAC (44–46). Ramachandran analyses were carried out using MolProbity (47). All residues are in the favored and allowed regions of the Ramachandran plot. Data processing and refinement statistics are summarized in *SI Appendix, Table S1*. The atomic coordinates and structure factors have been deposited in the Protein Data Bank with accession codes 7Y11 for AtSFH5-Sec14 in complex with L- α -PA and 7Y10 for AtSFH5-Sec14 in complex with DPPA. The structural representations were prepared with PyMOL (<http://www.pymol.org>).

TEM Analysis. The seventh rosette leaves of Col-0, *sfh5*, *sfh7*, and *sfh5 sfh7* double mutant were cut into small pieces and fixed in 2.5% glutaraldehyde in phosphate buffer (pH 7.2) for 20 h at 48 °C. After fixation, tissue was rinsed and postfixed overnight at 4 °C in 1% osmium tetroxide in 0.1 M cacodylate buffer

(pH 7.0), then dehydrated in an ethanol series, infiltrated with a graded series of epoxy resin in epoxy propane, and embedded in Epon 812 resin. Ultrathin sections were stained in uranium acetate followed by lead citrate and observed with a TEM (Hitachi; 80 kV).

Measurement of Chlorophyll and Photosynthetic Activity. Amounts of chlorophyll a and b were quantified using N, N-dimethylformamide (48). Briefly, 100 mg seventh to ninth rosette leaves of wild type and various mutants were used and absorbance was measured at 664, 647, and 625 nm. Photosynthetic parameter of NPQ was measured with an Imaging PAM 101 (Watz, Germany) according to the manufacturer's instructions.

Chloroplast Isolation, Lipid Extraction, and Quantification. Chloroplasts were isolated according to previous description (49) with some modifications. Briefly, 23-d-old *Arabidopsis* seedlings were homogenized in 10 mL isolation buffer (0.3 M sorbitol, 5 mM MgCl₂, 5 mM ethylene glycol-bis (β-aminoethyl ether)-N,N,N',N'-tetraacetic acid (EGTA), 5 mM EDTA, 20 mM 4-(2-hydroxyethyl)-1-piperazineethanesulfonic acid (HEPES)/ potassium hydroxide (KOH), 10 mM NaHCO₃, pH 8.0) and filtered through a double layer of miracloth. Obtained homogenate was centrifuged and pellet was resuspended, which were then loaded onto a two-step Percoll gradient consisting of a bottom layer (3 mL) comprising 2.55 mL Percoll solution (Percoll/polyethylene glycol (PEG) 6000/Ficoll/BSA, 95/3/1/1, w/v) plus 0.45 mL gradient mixture (25 mM HEPES-NaOH, pH 8.0, 10 mM EDTA, 5% sorbitol, w/v) and a top layer (7 mL) comprising 2.94 mL Percoll solution plus 4.06 mL gradient mixture. Determination of chloroplast yield was carried out using a hemocytometer, and chloroplast intactness was verified by phase-contrast microscopy (Zeiss).

Chloroplast lipids were extracted according to previous description (50). Solvent was evaporated under nitrogen, and lipid extract was dissolved in CHCl₃/methanol/50 mM sodium acetate in water (300/665/35, w/v). For phospholipid analysis, samples were analyzed by flow injection using a Shimadzu CBM-20A Lite high performance liquid chromatography (HPLC) system (Kyoto, Japan) with a solvent mixture of 10 mM ammonium acetate in methanol. MS analysis was performed on a 5500 QTrap triple quadrupole mass spectrometer (AB Sciex) equipped with a Turbo V electrospray ion source. For galactolipids, analysis was carried out using the HPLC system coupled with ion mass spectrometer X500 equipped with an ESI source (AB Sciex). Lipids were separated in a solvent of methanol/acetonitrile/water (2:2:1, v:v:v) with 10 mM ammonium acetate (NH₄AC). MS data were collected using Analyst and processed using SCIEX OS (AB Sciex).

1. G. Hölzl, P. Dörmann, Chloroplast lipids and their biosynthesis. *Annu. Rev. Plant Biol.* **70**, 51–81 (2019).
2. A. P. Hertle *et al.*, A Sec14 domain protein is required for photoautotrophic growth and chloroplast vesicle formation in *Arabidopsis thaliana*. *Proc. Natl. Acad. Sci. USA* **117**, 9101–9111 (2020).
3. P. Jarvis *et al.*, Galactolipid-deficiency and abnormal chloroplast development in the *Arabidopsis* *MGD Synthase 1* mutant. *Proc. Natl. Acad. Sci. U.S.A.* **97**, 8175–8179 (2000).
4. C. Xu, J. Fan, W. Riekhof, J. E. Froehlich, C. Benning, A permease-like protein involved in ER to thylakoid lipid transfer in *Arabidopsis*. *EMBO J.* **22**, 2370–2379 (2003).
5. K. Awai, C. Xu, B. Tamot, C. Benning, A phosphatidic acid-binding protein of the chloroplast inner envelope membrane involved in lipid trafficking. *Proc. Natl. Acad. Sci. U.S.A.* **103**, 10817–10822 (2006).
6. B. Lu, C. Xu, K. Awai, A. D. Jones, C. Benning, A small ATPase protein of *Arabidopsis*, TGD3, involved in chloroplast lipid import. *J. Biol. Chem.* **282**, 35945–35953 (2007).
7. J. Fan, Z. Zhai, C. Yan, C. Xu, *Arabidopsis* TRIGALACTOSYLDIACYLGLYCEROLS interacts with TGD1, TGD2, and TGD4 to facilitate lipid transfer from the endoplasmic reticulum to plastids. *Plant Cell* **27**, 2941–2955 (2015).
8. S. Lev, Nonvesicular lipid transfer from the endoplasmic reticulum. *Cold Spring Harb. Perspect Biol.* **4**, a013300 (2012).
9. K. Hanada, Lipid transfer proteins rectify inter-organelle flux and accurately deliver lipids at membrane contact sites. *J. Lipid Res.* **59**, 1341–1366 (2018).
10. K. Garner *et al.*, Phosphatidylinositol transfer protein, cytoplasmic 1 (PITPNC1) binds and transfers phosphatidic acid. *J. Biol. Chem.* **287**, 32263–32276 (2012).
11. Y. J. Kim, M. L. Guzman-Hernandez, E. Wisniewski, T. Balla, Phosphatidylinositol-phosphatidic acid exchange by Nir2 at ER-PM contact sites maintains phosphoinositide signaling competence. *Dev. Cell* **33**, 549–561 (2015).
12. M. Connerth *et al.*, Intramitochondrial transport of phosphatidic acid in yeast by a lipid transfer protein. *Science* **338**, 815–818 (2012).
13. F. Yu *et al.*, Structural basis of intramitochondrial phosphatidic acid transport mediated by Ups1-Mdm35 complex. *EMBO Rep.* **16**, 813–823 (2015).
14. V. A. Bankaitis, C. J. Mousley, G. Schaaf, The Sec14 superfamily and mechanisms for crosstalk between lipid metabolism and lipid signaling. *Trends Biochem. Sci.* **35**, 150–160 (2010).

Positional Analysis of Acyl Chains in MGDG. Lipid extracts were solved in CHCl₃/methanol (1:1, v/v), and the regioisomeric position of fatty acyl chains in MGDG was analyzed according to the previous descriptions (37–39). Samples flow were injected using Shimadzu CBM-20A Lite HPLC system (Kyoto, Japan) with a solvent mixture of methanol/acetonitrile (1:1, v/v, 10 mM NH₄AC) and isopropanol including 10 mM NH₄AC, respectively. Regioisomer analysis was performed on a ZenoTOF 7600 MS with a fragmentation mode of EIEIO (AB Sciex). The ion source parameters were set as follows: source temperature, 200 °C; curtain gas, 35; collision-activated dissociation gas, 7; two ion source gases, 55/55; ion spray voltage, 5,500V; temperature, 450 °C; declustering potential, 80 V. TOF MRMHR was set as follows: electron beam current, 7,000 nA; Zeno threshold, 100,000 cps. MS data were collected using Analyst and processed using SCIEX OS (AB Sciex).

Accession Numbers. Sequence data in this article are provided in the *Arabidopsis* Genome Initiative databases under following accession numbers: *AtSFH5* (At1g75370, NM_001161000), *AtSFH7* (At2g16380, NM_127192), *MGD1* (At4g31780, NM_119327), *MGD2* (At5g20410, NM_122048), *MGD3* (At2g11810, NM_126865), *DGD1* (At3g11670, NM_111999), *DGD2* (At4g00550, NM_116279).

Data, Materials, and Software Availability. All study data are included in the article and/or *SI Appendix*. Atomic coordinates and structure factor files have been deposited in the RCSB Protein Data Bank (<https://www.rcsb.org/>) under <https://doi.org/10.2210/pdb7Y11/pdb> and <https://doi.org/10.2210/pdb7Y10/pdb>.

ACKNOWLEDGMENTS. We thank Dr. Guo-Zhang Wu (Shanghai Jiao Tong University) for constructive discussions, Xiao-Shu Gao, Xiao-Yan Gao, Ji-Qing Li, and Zhi-Ping Zhang (CAS Center for Excellence in Molecular Plant Sciences) for Microscopy and TEM technical support, and Prof. Huiru Tang (Fudan University) and Ms. Ting Liu (AB Sciex) for great help on lipid analysis. We thank all staff members of beamline BL17U at Shanghai Synchrotron Radiation Facility for assistance in data collection. Funding: The study was supported by the National Natural Science Foundation of China (91954206 to H.-W.X., 31920103010 to J.-W.W., 31870280 to H.-Y.Y., 91754201 to J.-W.W.).

Author affiliations: ^aState Key Laboratory of Genetic Engineering, School of Life Sciences, Fudan University, Shanghai 200438, China; ^bNational Key Laboratory of Plant Molecular Genetics, CAS Center for Excellence in Molecular Plant Sciences, Chinese Academy of Sciences, Shanghai 200032, China; ^cInstitute of Molecular Enzymology, School of Biology & Basic Medical Sciences, Suzhou Medical College of Soochow University, Suzhou 215123, China; and ^dShanghai Collaborative Innovation Center of Agri-Seeds, Joint Center for Single Cell Biology, School of Agriculture and Biology, Shanghai Jiao Tong University, Shanghai 200240, China

15. R. Holíč, D. Šťastný, P. Griáč, Sec14 family of lipid transfer proteins in yeasts. *Biochim. Biophys. Acta. Mol. Cell Biol. Lipids* **1866**, 158990 (2021).
16. J. Huang, R. Ghosh, V. A. Bankaitis, Sec14-like phosphatidylinositol transfer proteins and the biological landscape of phosphoinositide signaling in plants. *Biochim. Biophys. Acta* **1861**, 1352–1364 (2016).
17. A. Haselier, H. Akbari, A. Weth, W. Baumgartner, M. Frentzen, Two closely related genes of *Arabidopsis* encode plastidial cytidinediphosphate diacylglycerol synthases essential for photoautotrophic growth. *Plant Physiol.* **153**, 1372–1384 (2010).
18. A. A. Kelly *et al.*, Synthesis and transfer of galactolipids in the chloroplast envelope membranes of *Arabidopsis thaliana*. *Proc. Natl. Acad. Sci. U.S.A.* **113**, 10714–10719 (2016).
19. V. A. Bankaitis, J. R. Aitken, A. E. Cleves, W. Dowhan, An essential role for a phospholipid transfer protein in yeast Golgi function. *Nature* **347**, 561–562 (1990).
20. G. Schaaf *et al.*, Functional anatomy of phospholipid binding and regulation of phosphoinositide homeostasis by proteins of the sec14 superfamily. *Mol. Cell* **29**, 191–206 (2008).
21. C. Panagabko, M. Baptist, J. Atkinson, In vitro lipid transfer assays of phosphatidylinositol transfer proteins provide insight into the in vivo mechanism of ligand transfer. *Biochim. Biophys. Acta. Biomembr.* **1861**, 619–630 (2019).
22. R. Ghosh, V. A. Bankaitis, Phosphatidylinositol transfer proteins: negotiating the regulatory interface between lipid metabolism and lipid signaling in diverse cellular processes. *Biofactors* **37**, 290–308 (2011).
23. B. D. Sha, S. E. Phillips, V. A. Bankaitis, M. Luo, Crystal structure of the *Saccharomyces cerevisiae* phosphatidylinositol transfer protein. *Nature* **391**, 506–510 (1998).
24. B. K. Nelson, X. Cai, A. Nebenfuhr, A multicolored set of in vivo organelle markers for co-localization studies in *Arabidopsis* and other plants. *Plant J.* **51**, 1126–1136 (2007).
25. R. Ghosh *et al.*, Sec14-nodulin proteins and the patterning of phosphoinositide landmarks for developmental control of membrane morphogenesis. *Mol. Biol. Cell* **26**, 1764–1781 (2015).
26. M. Hagio *et al.*, Phosphatidylglycerol is essential for the development of thylakoid membranes in *Arabidopsis thaliana*. *Plant Cell Physiol.* **43**, 1456–1464 (2002).
27. Z. Wang, C. Benning, Chloroplast lipid synthesis and lipid trafficking through ER-plastid membrane contact sites. *Biochem. Soc. Trans.* **40**, 457–463 (2012).

28. J. Browse, N. Warwick, C. R. Somerville, C. R. Slack, Fluxes through the prokaryotic and eukaryotic pathways of lipid synthesis in the "16:3" plant *Arabidopsis thaliana*. *Biochem J.* **235**, 25–31 (1986).
29. C. W. Yu, Y. T. Lin, H. M. Li, Increased ratio of galactolipid MGDG: DGDG induces jasmonic acid overproduction and changes chloroplast shape. *New Phytol.* **228**, 1327–1335 (2020).
30. E. Dubots *et al.*, Activation of the chloroplast monogalactosyldiacylglycerol synthase MGD1 by phosphatidic acid and phosphatidylglycerol. *J. Biol. Chem.* **285**, 6003–6011 (2010).
31. P. Dörmann, I. Balbo, C. Benning, *Arabidopsis* galactolipid biosynthesis and lipid trafficking mediated by DGD1. *Science* **284**, 2181–2184 (1999).
32. S. E. Phillips *et al.*, Yeast Sec14p deficient in phosphatidylinositol transfer activity is functional in vivo. *Mol. Cell* **4**, 187–197 (1999).
33. C. J. Lupton *et al.*, The cryo-EM structure of the human neurofibromin dimer reveals the molecular basis for neurofibromatosis type 1. *Nat. Struct. Mol. Biol.* **28**, 982–988 (2021).
34. M. J. Phillips, G. K. Voeltz, Structure and function of ER membrane contact sites with other organelles. *Nat. Rev. Mol. Cell Biol.* **17**, 69–82 (2016).
35. T. Li *et al.*, A combinatorial reporter set to visualize the membrane contact sites between endoplasmic reticulum and other organelles in plant cell. *Front. Plant Sci.* **11**, 1280 (2020).
36. R. Aviram *et al.*, Lipidomics analyses reveal temporal and spatial lipid organization and uncover daily oscillations in intracellular organelles. *Mol. Cell* **62**, 636–648 (2016).
37. T. Baba, J. L. Campbell, J. C. Y. Le Blanc, P. R. S. Baker, Structural identification of triacylglycerol isomers using electron impact excitation of ions from organics (EIEIO). *J. Lipid Res.* **57**, 2015–2027 (2016).
38. T. Baba, J. L. Campbell, J. C. Y. Le Blanc, P. R. S. Baker, Ikeda, Quantitative structural multiclass lipidomics using differential mobility: Electron impact excitation of ions from organics (EIEIO) mass spectrometry. *J. Lipid Res.* **59**, 910–919 (2018).
39. J. L. Campbell, T. Baba, Near-complete structural characterization of phosphatidylcholines using electron impact excitation of ions from organics. *Anal. Chem.* **87**, 5837–5845 (2015).
40. L. Qu *et al.*, Plant casein kinases phosphorylate and destabilize a cyclin-dependent kinase inhibitor to promote cell division. *Plant Physiol.* **187**, 917–930 (2021).
41. H. Wang *et al.*, ORP2 delivers cholesterol to the plasma membrane in exchange for phosphatidylinositol 4,5-bisphosphate (PI(4,5)P₂). *Mol. Cell* **73**, 458–473 (2019).
42. J. Dong *et al.*, Allosteric enhancement of ORP1-mediated cholesterol transport by PI(4,5)P₂/PI(3,4)P₂. *Nat Commun.* **10**, 829 (2019).
43. A. J. McCoy *et al.*, Phaser crystallographic software. *J. Appl. Crystallogr.* **40**, 658–674 (2007).
44. G. N. Murshudov, A. A. Vagin, E. J. Dodson, Refinement of macromolecular structures by the maximum-likelihood method. *Acta Crystallogr. D Biol. Crystallogr.* **53**, 240–255 (1997).
45. P. D. Adams *et al.*, PHENIX: Building new software for automated crystallographic structure determination. *Acta Crystallogr. D: Biol. Crystallogr.* **58**, 1948–1954 (2002).
46. P. Emsley, K. Cowtan, Coot: Model-building tools for molecular graphics. *Acta Crystallogr. D Biol. Crystallogr.* **60**, 2126–2132 (2004).
47. V. B. Chen *et al.*, MolProbity: All-atom structure validation for macromolecular crystallography. *Acta Crystallogr. D Biol. Crystallogr.* **66**, 12–21 (2010).
48. R. Moran, Formulae for determination of chlorophyllous pigments extracted with N, N-dimethylformamide. *Plant Physiol.* **69**, 1376–1381 (1982).
49. S. E. Kubis, K. S. Lilley, P. Jarvis, Isolation and preparation of chloroplasts from *Arabidopsis thaliana* plants. *Methods Mol. Biol.* **425**, 171–186 (2008).
50. R. Welti *et al.*, Profiling membrane lipids in plant stress responses: Role of phospholipase D α in freezing induced lipid changes in *Arabidopsis*. *J. Biol. Chem.* **277**, 31994–32002 (2002).